AIDIC *Conference Series*, Vol. 10, 2011
Editor Sauro Pierucci
DOI: 10.3303/ACOS1110017

ISBN 978-88-95608-58-7 ISSN 2036-5969

SIZE-SELECTED TiO2 NANOPARTICLES AS NBBs FOR NEW NANOSTRUCTURED FUNCTIONAL MATERIALS

Pavlo Gorbovyi, Zixian Jia, Mohamed Bouslama, Siteng Tieng, Mamadou Traoré, Mounir Ben Amar, Mohamed Amamra, Khay Chhor, Luc Museur[1], Andréi Kanaev*

Laboratoire des Sciences des Procédés et des Matériaux, UPR 3407 CNRS
[1] Laboratoire de Physique des Lasers, UMR 7538 CNRS
Université Paris 13, 99 avenue Jean-Baptiste Clément, 93430 Villetaneuse, France
* andrei.kanaev@lspm.cnrs.fr

We report on a new approach to the nanoparticulate materials preparation. The method is based on size-selective fabrication of chemically active metastable titanium-oxo-alkoxy nanoparticles in a sol-gel reactor with rapid (turbulent) micromixing, followed by their deposition as nanocoatings, impregnation into porous matrixes and consolidation into organic-inorganic hybrids. A striking feature of these materials is their extremely large specific-area interface. The related properties are reviewed.

Key words: nanoscience and nanotechnology, sol-gel process, oxide nanoparticles, nanostructured solids, electronic properties.

1. INTRODUCTION

Nanoparticulate and nanostructured oxides attract significant interest recent years (Rodriguez et al., 2007, Merhari, 2009). Many progresses have been achieved in synthesis of these materials and understanding of their structural and electronic properties. The elaboration process is generally found crucial to their electronic properties. In particularly, electronic structure and electron transport depend on the nature and extend of the inorganic interface, which can be tailored through the materials chemistry and processing. Moreover, the size of the building unit can affect the electronic band structure and related optical properties (Jortner, 1992). In these conditions, inadequate elaboration process resulted in a broad particle-size distribution may screen the size-specific effects and result in poor or non-optimised electronic materials.
Last years, our group has proposed the elaboration process of size-selected oxide nanoparticles in macroscopic quantities (grams) (Rivallin et al. 2005a; Azouani et al., 2007; Azouani et al., 2010a). The prepared oxo-alkoxy nanoparticles are methastable: because of their high chemical reactivity, they tend to aggregation and survive only in strictly controlled experimental conditions. This relative inconvenience make them however suitable for reactive doping (cationic and anionic) and capable forming strong covalent bonds with surface hydroxylated sites of supporting materials (Azouani et al., 2010b; Tieng et al., 2011a; Benmami et al., 2006; Bouslama et al., 2011).
The aim of this work is to describe an original elaboration process based on Nano Building Blocks (NBBs), which consists in selective fabrication of titanium-oxo-alkoxy nanoparticles in a sol-gel reactor, surface exchange and immobilisation. Different kind composite materials can be realised in this approach, which allows the material morphology control.

2. FABRICATION OF TiO_2 NANOPARTICULES

The sol-gel process presents an important approach for the fabrication of nanostructured materials in form of bulk solids and surface coatings (Brinker et al., 1990). However, difficulties in the process control and reproducibility are important due to a high chemical reactivity of the metal organic precursors (Livage et al., 1988). The nucleation stage is very rapid and accompanies the reagent mixing stage: as a result, local concentration variations are strong and starting conditions for the particle growth are poor defined, resulting in

Please cite this article as: Gorbovyi P., Jia Z., Bouslama M., Tieng S., Traore M., Ben Amar M., Amamra M., Chhor K., Museur L. and Kanaev A., (2011), Size-selected tio2 nanoparticles as nbbs for new nanostructured functional materials, AIDIC Conference Series, 10, 147-158 DOI: 10.3303/ACOS1110017

large particle size dispersion, which in term affects properties of the final materials (powders, coatings, bulk nanocomposites).
Mixing is a key parameter in tailoring the particle size distribution in industrial precipitation processes (Bałdyga et al., 1995), which becomes more and more critical when the particle reactivity increases and the particle size decreases. Important tools in this field are static mixers (Thakur et al., 2003), which have been studied last years in application to nanoparticles production (Gradl et al., 2006; Marchisio et al., 2006).
In this Chapter we present a background for the fabrication process of chemically active monodispersed titanium-oxo-alkoxy nanoparticules, suitable for chemical doping and deposition as macroscopic coatings and bulk nanocomposite solids.

2.1 Sol–Gel Reactor Equipped with a Rapid Mixer

The basic sol-gel chemistry involves hydrolysis-condensation reactions

$$...Ti-OR+H_2O \rightarrow ...Ti-OH+ROH \quad (1)$$

$$...Ti-OH+HO-Ti... \rightarrow ...Ti-O-Ti...+H_2O \quad (2)$$

which kinetics critically depends on the chemical concentrations. In particularly case of the TTIP (titanium-tetra-iso-propoxyde, $Ti(O^i\mathrm{Pr})_4$) precursor, the induction kinetics show strongly non-linear behavior: (Soloviev et al., 2003):

$$\tau_{ind}^{-1} = const \cdot C_{Ti}(H-H^*)^5 \quad (3)$$

where τ_{ind} is the induction time and H^*=1.45 stands for the critical hydrolysis ratio ($H = C_{H_2O}/C_{Ti}$). An explanation of this behavior has been given in later works by Rivallin et al. (2005a, 2005b). The nucleation stage is very short and is completed on the timescale of ~1 s. Strong local inhomogeneity of reagent concentrations at the fluid eddies boundaries during mixing results in a strong polydispersity of the obtained sols: e.g. large nanoparticles with the condensation ratio k=n(O)/n(Ti)~1.18 appear at H~0.2 (Blanchard et al., 2000). Perfect starting conditions of the sol-gel process consist in homogenizing local fluid composition faster than the reactions (1)-(2) begin, i.e. on the timescale of 0.01 s or even shorter.
The sol–gel reactor presented in Figure 1 permits the rapid fluids micromixing. It consists of two thermostatic containers of 0.05 dm^3 volume each, fed with TTIP/2-propanol and H_2O/2-propanol solutions (*Interchim*).

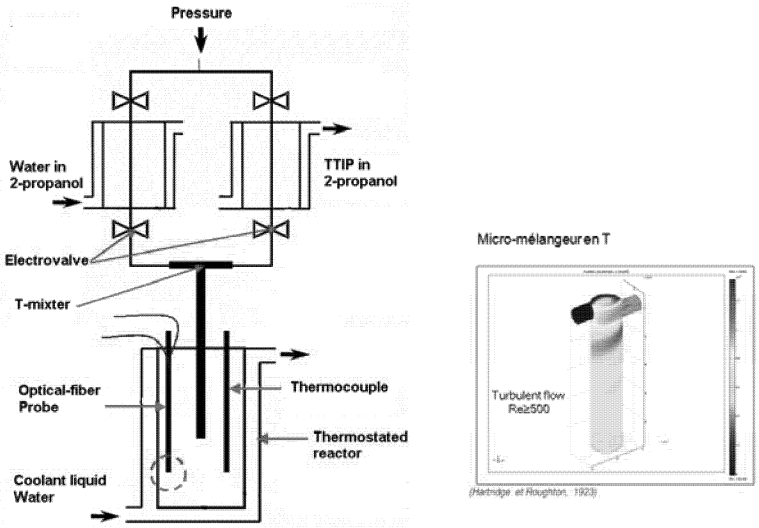

Figure1: A sketch of the sol-gel reactor (left) and its T-mixer (right). Blue (water) and red (TTIP) inputs transform after perfect mixing into the blue-green output (right).

The reactor temperature was controlled by a thermo-cryostat (Haake, DC10K15). The solutions are injected into the reactive volume the static T-shaped mixer (Hartridge and Roughton, 1923) by applying the dry-N_2 gas

pressure at a synchronous opening of the electro-valves. After the injection, the sol-gel process occurred in the thermostatic reaction volume.

The mixing process can be considered at two scales. At the macroscopic scale, it was described using a two-fluid model that distinguishes the fluids coming from each of the two feeding arms of the T-mixer. The macro-mixing of these fluids takes place through the eddies diffusion. The corresponding diffusion coefficient is estimated from

$$D_t = c\left(\frac{\varepsilon}{\nu}\right)^{1/2} \tag{4}$$

where ν is the kinematic turbulent viscosity, ε is the specific dissipated turbulent power and *c* is a geometrical constant. The dynamic turbulent viscosity is given by

$$\eta = \frac{\rho C_\mu k^2}{\varepsilon} \tag{5}$$

where *k* is the kinematic turbulent energy and C_μ is a model constant set to 9×10^{-2} in this work. The local micro mixing takes place over a characteristic length scale corresponding to the Kolmogorov length, which defines the size of the elementary eddies in the fluids. Using a simple mixing model, the Kolmogorov length can be expressed as

$$L_k = \left(\frac{\nu^3}{\varepsilon}\right)^{1/4} \tag{6}$$

In order to determine the micro mixing quality one has to estimate the space distribution of L_k and consequently ν and ε. Transport equations were solved in the frame of the Reynold Averaged Navier–Stokes model describing the turbulences in terms of *k* and ε (Bird et al., 2001; Ferziger and Peric, 2002) by using commercial software fluidyn-NSNT developed by *Transoft International*. Our estimations based on confrontation between the modeling and measurements confirm that high Reynold's numbers of $Re\geq4.5\cdot10^4$ ($Re=4Q\rho/\pi\eta d$, where Q, ρ, and η are the fluid flow rate, density and dynamic viscosity) the turbulent flow installed resulted in the reagents mixing on a molecular level occurred within several milliseconds, which is shorter than that of primary hydrolysis-condensation reactions (1)-(2). Indeed, both measured mean size and dispersion of nanoparticle show minima in these conditions (Rivallin et al., 2005a; Azouani et al., 2010a). This regime corresponds to small Damköhler numbers: $Da=\tau_{phys}/\tau_{chem}\leq1$, which is a general precondition to achieve the narrowest particle size distribution (Bałdyga et al., 1995).

2.2 In-situ particle size measurements

DLS/SLS is a widely used technique to characterize stable colloidal particles. Complementary information about fractal dimension of the growing nanoparticles can be obtained from both intensity (SLS) and particle size (DLS) measurements. We have developed an optical fiber probe to perform particle size measurements in a precipitation reactor, allowing easy access with a laser beam to its different points (figure 2a). This probe was essential in the reactor control because direct dynamical and static light scattering (DLS/SLS) measurements using classical experimental geometry (tracing of the beam with lenses) are influenced by a macroscopic movement of the reactor fluid and require optical-quality entrees in the reactor walls. Moreover, the small interaction volume (figure 2b) considerably weakens a probability of the multiple-scattering events even at high colloid concentrations. It was shown that despite of a lower coupling efficiency with the laser beam, use of the monomode optical fibre results in higher contrast of the autocorrelation function and shorter accumulation time, which guarantees desirable precision of measurements.

Measurements of the autocorrelation function (ACF) provided the diffusion coefficient, which was related to the hydrodynamic particle radius by the Stokes–Einstein equation (figure 2c). The experimental geometry with a right angle between laser beam and the receiver (photo-multiplier, PM) was generally used. We used two probes made from a couple of monomode (core diameter 5 mm, numerical aperture 0.1) and multimode (100 μm, 0.3) optical fibers supplied by SEDI. The fibres of each couple were fixed at right angles and at a distance of 1.5 mm between the light ends. The laser radiation was coupled to one of the fibers (sender) using the optical fiber

adapter (Newport), and the second fiber (receiver) transmitted the scattered laser radiation to PM. The ACF measurements were achieved using a CUBE 640-40 CIRCULAR laser (Coherent), in the homodyne technique of photon-correlation spectroscopy by using a 16-bit, 72-channel digital correlator (PhotoCor Instruments). The probe calibration has bee performed with 100-nm latex particles.

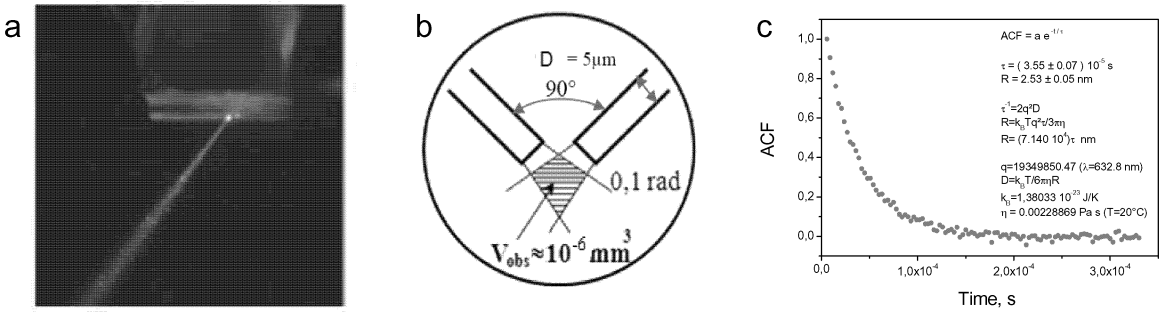

Figure 2: Image (a) and sketch (b) of the fiber-optical probe and measured ACF at C_{Ti}=0.15M, H=2.0, T=20°C (c)

2.3 Selective preparation of titanium-oxo-alkoxy nanoparticles

As Azouani et al. (2007) have shown, three kind of size-selected nanoparticles can be generated in the reactor, with hydrodynamic diameter of 2.0, 3.2 and 5.2 nm: the first two were called clusters and the last one - nuclei. The nanoparticles have metal oxide core and surface propoxy and hydroxy groups. Moreover, it was shown that the nuclei appeared only at hydrolysis ratio H≥2; they subject to the accelerated growth by aggregation, presented by well-known induction kinetics expressed by equation (3). At H=2.0 the induction kinetics slow down and the induction time tends to infinity. This point is most favorable for generation and deposition of metastable 5.2-nm nanoparticles, which growth is inhibited because of the fluid composition and temperature control in the sol-gel reactor: it was used below for preparation of the composite and hybrid materials. The reactor was operating at temperature of 20.0 °C. TTIP of 98% purity, 2-propanol (Interchim), and distillated water were used.

3. FABRICATION OF SILVER-TIO_2 NANOCOMPOSITES

Silver and gold nanomaterials display unique optical properties making them interesting for chemical and biological sensing and information technologies (Maier, S. A. 2007; Brongersma and Kik, 2007) but also for solar energy conversion (Ferry et al., 2010) and photocatalysis (Awazu et al., 2008; Morfa et al., 2008). A combination of heterogenous catalysts with non-thermal plasma is a promising technology for gaseous effluents treatment, characterized by high efficiency, high mineralization rates and low by-products formation. The insertion of noble metals, such as Ag, Pt and Au into TiO_2 coatings may provide two types of enhancement effects on the VOCs degradation; one related to the photocatalytic activity of titania, and the other one related to the thermocatalytic activity of metals. Optimisation of the process requires narrow polydispersity and morphology control of the nanofimls. In this chapter we describe the fabrication of the nanoparticulate Ag-TiO_2 coatings.

3.1 Preparation of nanoparticulate Ag-TiO_2 films

The 5.2 nm sol particles of total mass of 1.15 g per reactor run were generated in 2-propanol solutions of 20 °C with TTIP at concentration C_{Ti}=0.146M and hydrolysis ratio H=2.0. As explained above, the particles nucleation takes place in these conditions, however their agglomeration is suppressed. Thin glass plates of size 24x60x0.16 mm preliminary treated in acid solution were dip-coated with the reactor solution under dry nitrogen gas flow (relative ambient humidity <10%). The withdrawing speed of the substrates was 4 mm/s. An additional rinsing with dry alcohol was used to remove liquid layer on the surface of the plates containing excessive nanoparticles. The covered plates were dried in the glove box overnight and subsequently in an oven at 80 ° C for 24 hours.

Only nanoparticles reacting with surface hydroxyls remain on the surface after the deposition process. As a result, nanoparticulate films were produced by chemical deposition in form of the monolayer nanoparticles on glass plates (Benmami et al., 2006).
The silver ions solution was prepared by dissolving 0.725g of $AgNO_3$ salt in 15 mL of deionized water (solution A). Then 1ml of solution A was added to 50 ml of 2-propanol under vigorously stirring in the dark (solution B). The solution B was cast on TiO_2 nanoparticulate film prepared on the previous step. The titania film was illuminated with UV light (8W, PHILPS, 360 nm) from the distance of 35 mm for different periods of time resulting in the photocatalytic reduction of Ag^+ ions on the TiO_2 nanoparticles. An additional rinse with deionized water is done at the end in order to remove the remaining solution. The glass plates are then dried in an oven at 80 ° C.

3.2 Morphology of nanoparticulate Ag-TiO_2 films

The SEM images of the prepared Ag-TiO_2 nanoparticulate coatings are shown in Figure 3(a,b) after 1 and 10 min illumination. Both size and number density of silver nanoparticles (NPs) increase with the illumination dose. A blanc text conducted on glass plates without the TiO_2 layer has evidenced no silver NPs.

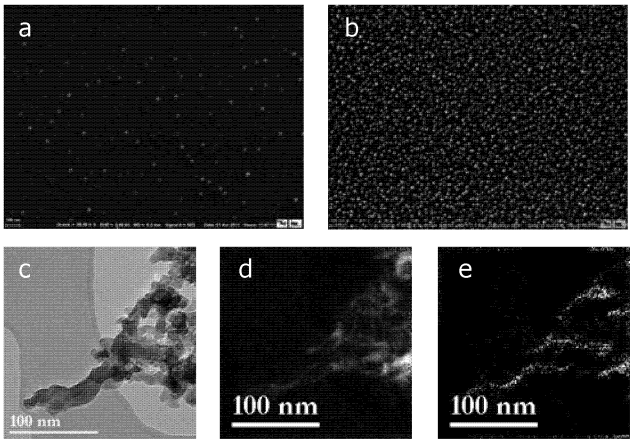

Figure 3: SEM images of Ag grown on TiO_2 NP coating after illuminating (λ≈360 nm) for 1 min (a) and 10 min (b). HRTEM image of Ag grown on TiO_2 NPs deposited on UPA (c) and EF-HRTEM Ti (d) and Ag (e) maps (360 nm, 1 min).

The results show that the size of Ag NPs grown on the nanoparticulate titania is limited by ~15 nm. Larger Ag NPs can be produced by percolation of these surface structures. High resolution electron microscopy (HRTEM) and energy-filtered HTRM (EF-HTRM) images in Figure 3(c-e) realised Ag NPs grown on the TiO_2 nanoparticules impregnated into ultraporous alumina matrixes (see Chapter 4) confirm that the metal reduction takes place on the titania surface. Whether spherical Ag NPs appear as a result of the surface atoms coalescence or percolation as a surface layer remains unclear. The Ag-TiO_2 composite coatings exhibit strong plasmon resonances, which brightness and surface density increases with the Ag NPs density. The study is under way to elucidate the mechanism of the NPs growth and the morphological changes of the structures.

4. DEPOSITION OF TiO_2 NANOPARTICLES INTO ULTRA-POROUS MONOLYTHIC ALUMINA

A fabrication of non-agglomerated nanoparticulate solids with an open structure is a chalenging task in field of nanotechnology and nanomaterials. Such solids would permit concerving specific size-selected physical and chemical properties and highest specific area of the active phase, by avoiding health problems related to undesirably nanoparticles inhalation. One of most important classes of functional nanomaterials are metal oxides with application in fields of the environmental protection (gas/water cleaning technologies: photocatalysis, adsorption).

Indeed, the tendency of oxide nanoparticles towards agglomeration is very strong and most of the existing methods for the nanoparticles mass-production results in powder-like products with μm-size aggregates of the primary nanoparticles. Their individual responses are often found strongly inhibited in these conditions. The solution can be found in preparation of ultraporous nanostructured monolyths, mechanically stable, with high internal volume and specific area, and capable incorporating spatially separated nanoparticles of a large total mass. Ultraporous monolythic alumina (UPA) reply this criteria. Below we describe the TiO_2NPs-UPA composites preparation and present their remarkable structural and photocatalytic properties.

4.1 Elaboration of ultra porous alumina

The UPA monoliths were grown (~1 cm/hour) by oxidation of high-purity metallic aluminium (99,999%) in humid atmosphere trough a mercury-silver layer (Vignes et al., 2004; 2008). The raw UPA monoliths have porosity >99% and specific surface area of ~300 m^2/g. The microstructure of this very hydrated material (40 wt % of water), consists of tangled alumina fiber with a diameter of ~5 nm. Chemical and thermal treatments were used to increase its mechanical rigidity. The monolith alumina crystallization goes through the following steps:

- At temperatures above 870 °C γ-alumina polymorph appears.
- At 1150°C, it turns into θ-alumina with the average grain size of ~10 nm and specific area ~ 110 m^2/g.
- At 1200-1250°C, transformation into α-alumina occurs, leading to a microstructure with a 200-300 nm grain size and specific area of 5-10 m^2/g.

The high porosity of the raw monoliths allows a rapid and homogeneous impregnation of gaseous species. A remarkable modification of the alumina has been obtained when a low amount of silica (about 6 wt%) is incorporated into the UPA using trimethylethoxysilane (TMES: $(CH_3)_3$-Si-C_2H_5O) hydrolyzing at the hydrated surface. The silica addition delays the transformation into α polymorph up to 1400°C. This chemical modification stabilizes alumina with a high specific surface area at a higher temperature (Mazerolles et al., 2003). E.g. the UPA specific area is 170-180 m^2/g after heating at 1150 °C, and about 110 m^2/g after heating at 1300°C.

4.2 Preparation of nanocomposites

The TiO_2NPs-UPA nanocomposites were prepared by impregnation of 5.2 nm titanium-oxo-alkoxy nanoparticles into the porous θ alumina. These prepared NPs are most suitable for impregnation, since they are chemically active capable forming strong covalent bonds with surface hydroxylated sites of the matrix. Their *in situ* thermal treatment permits elimination of residual organics and crystallization.

For impregnation, the alumina monolith was cut into pellets of 2-5 mm size and introduced into the thermostated reactor bath with the reactive metastable colloid. The colloid fills the porous pellets at short contact and the contained nanoparticles react with surface hydroxyls of the matrix. The pellets are then withdrawn from the reactor and dried overnight at 80 °C. This procedure can be repeated several times in order to increase the loaded TiO_2 mass. The TiO_2NP-UPA composite was thermally treated in the temperature range between 400 and 1200°C for 4 hours. This treatment does not alter the alumina matrix previously treated at 1300 °C, but triggered TiO_2 transformation from amorphous to anatase and finally to the most stable rutile polymorphs.

4.3 Structural characterization of nanocomposites

The composites were prepared based on TMES-treated UPA calcinated at 1300 °C of θ polymorph. The specific area of the composite material does not decrease after the NPs impregnation, as summarized in Table 1. These results show that the material conserves its open structure and that no pores closure appears at the NPs impregnation.

Table 1: Cristalline phase and specific surface area of UPA after annealing σ_a and NPs impregnation σ_c.

T (°C) treatment	Polymorph phase	$\sigma_a(m^2/g)$	$\sigma_c(m^2/g)$
1300	θ	110	115

The extremely low density and high porosity of the monolithic alumina make them interesting for applications as adsorbing matrixes (di Costenzo T. et al., 2004). Considering the impregnation corresponding to one TiO_2 NPs monolayer, the theoretical estimate for the inner surface coverage results in the maximum mass loading of 110 wt.%; more than a half of the composite mass may be in form of nanoparticles. The deposited TiO_2 mass was measured by ammonium sulphate NH_4SO_4 - sulfuric acid H_2SO_4 digestion method (Coronado et al., 2003). Typically, 9 wt.% of the TiO_2 NPs were put into the UPA(θ) matrix at one impregnation cycle; consequently after three impregnation cycles the nanoparticles constitute about 26 wt.% of the composite material.
After the impregnation, the NPs are well dispersed in UPA (figure 4a,b). An isolated 5-nm TiO_2 nanoparticle can be seen on the energy filtered HRTEM image in figure 4c. Strong covalent Ti-O-Al bonds may be a reason of an apparent deformation of the deposited nanoparticle.

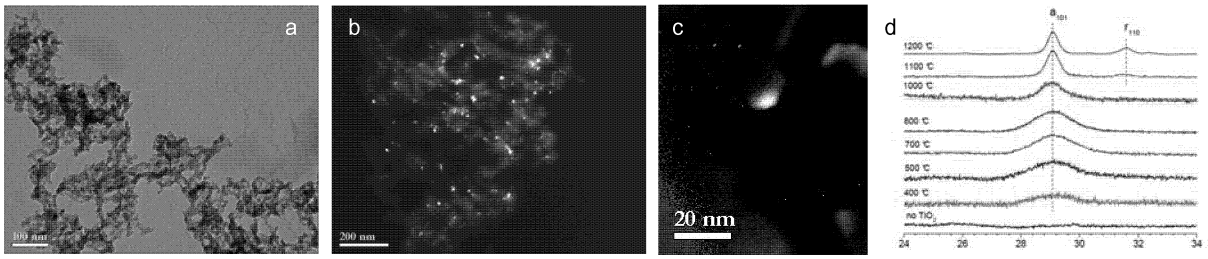

Figure 4: HTRM (a) and EF-HRTEM (Ti) images of the prepared nanocomposite and its X-ray diffraction patterns ($\lambda_{CoK\alpha}$=1.789 A) after its thermal treatment between 400 and 1200 °C.

More support to the above conclusion about weak nanoparticles aggregation in the composite sample with (3 impregnations) can be found in the XRD patterns, which are shown in Figure 3d in the range of the main anatase 101 and rutile 110 picks. In fact, it is known that the aggregated powder-like TiO_2 nanoparticles rapidly increase their crystalline domain at temperatures above 350 °C and the transformation from anatase to rutile phase begins appreciably at temperatures above 600 °C (Zhang and Banfield, 2000). Moreover, the very slow transformation ≤1%/h has been observed at even lower temperature of 465°C (Gribb and Banfield, 1997). In contrast, the nanoparticles deposited onto the UPA do almost not increase the size until temperatures as high as 800 °C; the rutile phase appears only at temperatures as high as 1100 °C. This phenomenon is explained by thermally-activated surface diffusion, which accelerates nanoparticles aggregation and thereafter growth of the crystalline domains. According to Zhang and Banfield (1998) anatase becomes more stable than rutile when TiO_2 particle size decreases below ca. 14 nm. Therefore, the strong increase of the phase transition temperature from 600 to 1100°C provides evidence of the agglomeration suppression. Indeed, according to the Gaussian fit by Scherrer formula (solid lines in figure 4d), the crystalline TiO_2 size is ~5 nm in the temperature range below 800 °C, and it is about 17 nm at 1100 °C when the rutile phase becomes observable. The size of rutile domains at 1100 °C is ~5 nm, which suggests its nucleation onto the anatase nanoparticle.
Our observation support earlier conclusions about titania polymorphs stability. They also show an exceptional stability of the TiO_2NPs-UPA nanocomposites against the nanoparticles agglomeration; the last allows considering these media for novel functional nanostructures with macroscopic response identical to that of its constituting nanometric unit.

4.4 Photocatalytic activity of nanocomposites

The photocatalytic activity of the prepared TiO_2NPs-UPA nanocomposites was meassured in a continuous-flow fix-bed reactor (Tieng et al., 2011b) using ethylene gas (36 ppm) mixture with dry air (1 atm, 85 ml/min). The gas passes through a reactor tube of 6-mm diameter transparent in UV-A spectral range. The tube is filled with the photocatalyst pellets. The tube is surrounded at a radial distance of 3 cm by six 8-W lamps emitting at 362 nm. Ethylene concentrations before (C_{in}) and after (C_{out}) the photocatalytic reactor were monitored by on-line gas chromatography (Varian CP 3800). The specific reactivity of the photocatalyst $r_S = [ln(C_{in}/C_{out})]/m_{TiO_2}$, was obtained by normalisation of the product Rτ on the deposited titania mass (g). This value was used as a direct measure of the material activity since the reactor geometry, lamp intensity and the pollutant residence time in the reactor (3.0 s) were kept constant in the experiments.

As our results have shown (Bouslama et al., 2011), the specific reactivity r_S of the TiO_2NPs-UPA(θ) nanocomposites increases with both mass of the deposited TiO_2NPs and temperature of thermal treatment until 600 °C. On the other hand, further increase of the temperature results in a weak decrease of r_S (by 40% in the range from 500 to 1000 °C) takes place. This result is presented in figure 5 along with the anatase particle size extracted from the XRD measurements (figure 4d) and the rutile fraction F_r in the catalyst calculated according to $F_r = 1-(1+1.265 I_{r110}/I_{a101})^{-1}$. The specific reactivity r_S does not vary appreciably and decreases slowly by only 40% in the range from 500 to 1000 °C; on the other hand, it strongly decreases by a factor of 30 at T=1200 °C. The initial smooth decrease of r_S at T≤1000 °C may be related to the electron localization radius while the strong decrease at T>1000 °C to the rutile appearance.

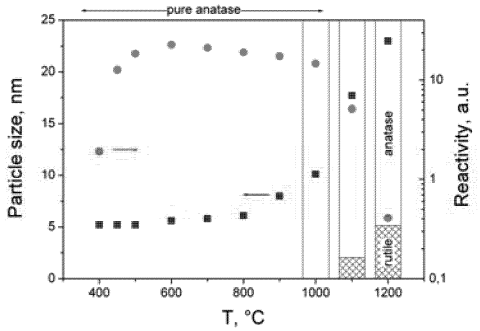

Figure 5: Specific reactivity r_S (a) and TiO_2 particles size of the photocatalyst (Bouslama et al., 2011) .

5. HYBRID ORGANIC-INOGARNIC MATERIALS

Last decades, organic-inorganic hybrid materials were intensively development (Gómez-Romero and Sanchez, 2003; Kickelbick, 2006; Merhari, 2009; Sanchez et al., 2010). Titanium dioxide hybrids attract a particular interest due to their high refractive index, biocompatibility and electron transport properties. Exceptional electronic properties of these hybrids are related to the photoinduced electon-hole separation and storage by the inorganic component (Kameneva et al., 2005; Kuznetsov et al., 2009). Recently, the most high charge separation efficiency of 50% and loading capacity of ~10% Ti atoms have been reported in the nanoparticulate hybrids (Gorbovyi et al., 2011).

Below we describe the elaboration method for new electronic materials: nanopparticulate polymer-TiO_2 hybrids. Their nano building blocks (NBBs) serve to be size-selected 5-nm titanium-oxo-alkoxy nanoparticles generated in the sol-gel reactor described in Chapter 2. These hybrids permit realization of 3D-microstructures, which conserve their high photonic sensitivity.

5.1 Experimental elaboration

Our approach to fabrication of nanoparticulate organic-inorganic hybrids consists in generation of monodispersed TiO_2 NPs, followed by their chemical surface modification, concentration adjustment, and consolidation into the polymer matrix. The sol particles were generated in 2-propanol solutions with TTIP at concentration C_{Ti}=0.15 M and hydrolysis ratio H=2.0 at T=20.0 °C. Two polymerisable monomers, MAPTMS (methacryloxy-propyl-trimethoxysilane) and HEMA (2-hydroxyethyl methacrylate), were used for replacement of the surface propoxy groups. The monomers were preliminary distillated in order to eliminate impurities and traces of spontaneous polymerization inhibitors. The solvent exchange is performed by monomer addition to 2-propanol/TiO_2 nanocolloid under stirring and vacuum pumping through the LN trap overnight. The 2-propanol elimination has been controlled by Raman spectroscopy. The NPs loading in the hybrid material can be adjusted at this stage by evaporating more alcohol than adding monomers: the maximum Ti concentration of 3.0 M has been achieved. The polymerization of this new nanoparticulate precursor was realized both thermally with addition of the AIBN initiator and by photons with an addition of a photoinitiator. 2D and 3D structures were realized by 3rd harmonics Nd:Yag laser (355 nm) and femtosecond Ti:sapphire laser system (800 nm) respectively.

5.2 Results

The exploitation of the ACF curves of the 1.5 mol/l MAPTMS-TiO_2 colloid shows that the NPs radius is conserved after the solvent exchange. This shows that the solvent exchange can be completed without changing the particle's size and aggregation state. Recently, Gorbovyi et al. (2010) have demonstrated that the surface ligands replacement $O^iPr \rightarrow$OEMA results in the Class II hybrids with strong covalent bonds between the constituting organic and ionorganic components. In the same time, the ligand's exchange between MAPTMS and 2-propanol groups leading to the creation of covalent Si-O-Ti bonds cannot been evidenced: indeed, the characteristic vibration band at 939 cm^{-1} was not appeared in the FTIR spectra. The pMAPTMS-TiO_2 hybrids were supposed to be bound by weak Van-der-Waals forces, which is characteristic of the Class I hybrids.

Organic polymerization of the nanoparticulate precursor at temperatures below 90°C results in non-colored transparent solids. It was monitored by observing characteristic Raman and FTIR vibrational peaks of C=C (1641 cm^{-1}), C=CH_2 (1407 cm^{-1}) and C-CH (1450 cm^{-1}) (Mabilleau et al, 2008). Figure 6 clearly shows vanishing of the C=C band intensities and increase of that of the C-C band, which indicates the elongation of the polymeric chains (figure 6). In the same time, our measurements show that some residual non-polymerised monomers remain in the hybrids with the increase of the nanoparticules loading.

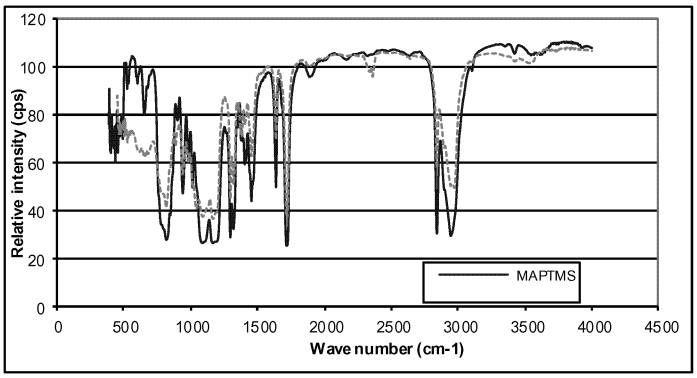

Figure 6: FTIR spectra of MAPTMS and sol of TiO_2 nanoparticules (C_{Ti}=3.0 M)

Figure 7 shows two kinds of photonic structures realized at LZH e.V. (Germany) by 2-photon laser polymerization technique. The hybrids conserve their photocromic properties, permitting laser micropatterning as described by Fadeela et al. (2006).

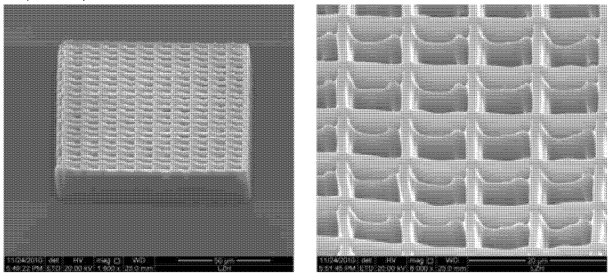

Figure 7: Laser polymerisation microstructuring of realysed on the pMAPTMS-TiO_2 hybrids at LZH e.V.

Indeed, the nanoparticulate hybrids obtained by both thermal and laser polymerization darken when they irradiated by UV-A light. The photochromism has been assigned to shallow polaronic Ti^{3+} centers formed owing to CB-electron trapping on Ti^{4+} (Kuznetsov et al., 2009). We have measured the photonic sensitivity of the prepared hybrids in pump-probe experiments using nanosecond UV laser (355 nm) with fluences of 10 mJ/cm^2. The darkening curve is presented in figure 8. It evidences the photoinduced charge separation efficiency in pMAPTMS-TiO_2 hybrids $\eta=dN_{Ti3+}/dN_{ph}$=6 % and charge storage capacity of $Q=N_{Ti3+}/ N_{Ti3+}$=6 %. Compared to pHEMA-TiO_2 hybrids with η=50 % and Q=12% (Gorbovyi et al., 2010), the pMAPTMS-TiO_2 hybrids seem to be less efficient.

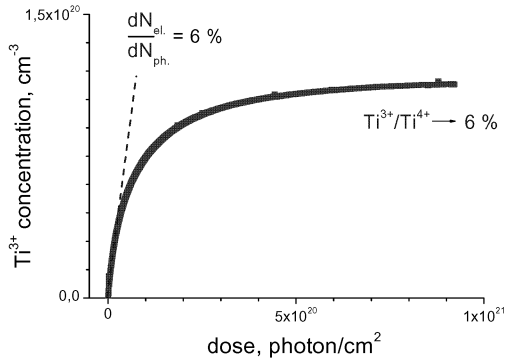

Figure 8: Darkening kinetics of MAPTMS-TiO_2 hybrids (C_{Ti}=3.0 M).

6. CONCLUSIONS

In conclusion, we present a new approach to the nanoparticulate composite materials preparation. It is based on size-selective fabrication of chemically active metastable titanium-oxo-alkoxy nanoparticles (in gram quantities) in a sol-gel reactor with rapid (turbulent) micromixing, followed by their chemical deposition. The method permits avoiding nanoparticles agglomeration, which is a general problem of nanomaterials and nanotechnology screening size-specific effects and resulting in poor or non-optimised electronic materials.

We have presented three examples of realized nanoparticulate macroscopic solids: photocatalytic TiO_2 and plasmonic Ag-TiO_2 nanocoatings, TiO_2NP-UPA composites, and photochromic organic-inorganic hybrids. They exhibit strong photonic sensitivity, promising for large-scale environmental applications.

7. REFERENCES

Awazu K., Fujimaki M., Rockstuhl C., Tominaga J., Murakami H., Ohki Y., Yoshida N., Watanabe T., 2008, A plasmonic photocatalyst consisting of silver nanoparticles embedded in titanium dioxide, J. Am. Chem. Soc. 130, 1676-1680.

Azouani R., Soloviev A., Benmami M., Chhor K., Bocquet J.-F., Kanaev A., 2007, Stability and growth of titanium-oxo-alcoxy $Ti_xO_y(O^iPr)_z$ clusters, J. Phys. Chem. C 111, 16243-16248.

Azouani R., Michau A., Hassouni K., Chhor K., Bocquet J.-F., Vignes J.-L., Kanaev A., 2010a, Elaboration of pure and doped TiO_2 nanoparticles in sol-gel reactor with turbulent micromixing: application to nanocoatings and photocatalysis, Chemical Engineering Research & Design, 88, 1123-1130.

Azouani R., Tieng S., Chhor K., Bocquet J.-F., Eloy P., Gaigneaux E. M., Klementiev K. and Kanaev A. V., 2010b, TiO_2 doping by hydroxyurea at the nucleation stage: towards new photocatalyst in the visible spectral range, Phys. Chem. Chem. Phys. 12, 11325-11334.

Benmami M., Chhor K., Kanaev A., 2006, High photocatalytic activity of monolayer nanocoatings prepared from non-crystalline titanium oxide sol nanoparticles, Chem. Phys. Lett. 422, 552-557.

Blanchard J., Ribot F., Sanchez C., Bellot P. V., Trokiner A., 2000, Structural characterization of titanium-oxo-polymers synthesized in the presence of protons or complexing ligands as inhibitors, J. Non-Cryst. Solids, 265, 83-97.

Bouslama M., Amamra M., Tieng S., Brinza O., Chhor K., Abderrabba M., Vignes J.-L., Kanaev A., 2011, Isolation of titania nanoparticles in monolithic ultraporous alumina: effect of nanoparticle aggregation on anatase phase stability and photocatalytic activity, J. Appl. Catal. A 402, 156-161.

Bałdyga J. and Pohorecki R., 1995, Turbulent micromixing in chemical reactors - a review. Chem Eng J, 58, 183-195.

Bird R. B., Stewart W. E., Lightfoot E. N., 2001, Transport Phenomena, John Wiley & Sons.

Brinker C. J. and Scherer G. W., 1990, Sol-Gel Science - The Physics and Chemistry of Sol-Gel Processing, Academic Press.

Brongersma M. L. and Kik, P. G., Eds., 2007, Springer Series in Optical Sciences, vol. 131, Surface Plasmon Nanophotonics, Springer.

Di Costanzo T., Fomkin A. A., Frappart C., Khodan A. N., Kuznetsov D. G., Mazerolles L., Michel D., Minaev A. A., Sinitsin V. A., Vignes J.-L., 2004, New Method of Porous Oxide Synthesis: Alumina and Alumina Based Compounds, Mater. Sci. Forum 453-454, 315-322.

Coronado J. M., Zorn J. M., Tejedor-Tejedor I., Anderson M., 2003, Photocatalytic oxidation of ketones in the gas phase over TiO_2 thin films: a kinetic study on the influence of water vapour, Appl. Catalysis B 43, 329-344.

Fadeela E., Koch F., Chichkov B., Kuznestov A., Kameneva O., Biyurin N., Sanchez C., Kanaev A., 2006, Laser imprinting of 3D structures in organic-inorganic gel-based titanium oxide hybrids, Appl. Phys. A 84, 27-30.

Ferry V. E., Munday J. N., Atwater H. A., 2010, Design Considerations for Plasmonic Photovoltaics, Adv. Mater. 22, 4794-4808.

Ferziger, J.H. and Peric, M., (2002). *Computational Methods for Fluid Dynamics*. (Springer).

Gribb A. A. and Banfield J. F., 1997, Particle size effects on transformation kinetics and phase stability in nanocrystalline TiO_2, Am. Mineralogist, 82, 717-729.

Gorbovyi P., Uklein A., Tieng S., Traore M., Chhor K., Museur L., Kanaev A., "Novel nanostructured pHEMA-(oxo)TiO_2 hybrid materials with efficient light-induced charge separation", Nanoscale 3 (2011) 1807-1812.

Gorbovyi P., Uklein A., Kostrov A., Tieng S., Traore M., Brinza O., Chhor K., Museur L., Kanaev A., 2010, Elaboration et microstructuration laser des matériaux hybrides organiques-inorganiques photochromes à base de gels de TiO_2, Proc. MATERIAUX 2010, Nantes, France.

Gómez-Romero P., Sanchez C., 2003, Functional Hybrid Materials, Wiley.

Gradl J., Schwarzer H.-C., Schwertfirm F., Manhart M. and Peukert W., 2006, Precipitation of nanoparticles in a T-mixer: Coupling the particle population dynamics with hydrodynamics through direct numerical simulation. Chem. Eng. Process. 45, 908-916.

Hartridge H. and Roughton F. J. W., 1923, A method of measuring the velocity of very rapid chemical reactions. Proc. R. Soc. London A 104, 376–394.

Jortner J., 1992, Cluster Size Effects, Z. Phys. D 24, 247-275.

Kameneva O., Kuznetsov A. I., Smirnova L. A., Rozes L., Sanchez C., Alexandrov A., Bituyrin N., Chhor K., Kanaev A., 2005, New photoactive hybrid organic–inorganic materials based on titanium-oxo-PHEMA nanocomposites exhibiting mixed valence properties, J. Mater. Chem., 15, 3380-3383.

Kickelbick G., 2006, Hybrid Materials: Synthesis, Characterization and Applications, Wiley.

Kuznetsov A. I., Kameneva O., Bituyrin N., Rozes L., Sanchez C., Kanaev A., 2009, Laser-induced photopatterning of organic-inorganic TiO_2-based hybrid materials with tunable interfacial electron transfer, Phys. Chem. Chem. Phys. 11, 1248-1257.

Livage J., Henry M., Sanchez C., 1988, Sol-gel chemistry of transition metal oxides, Prog. Solid-State Chem. 18, 259-341.

Mabilleau G., Cincu C., Basle M. F., Chappard D., 2008, Polymerization of 2-(hydroxyethyl)methacrylate by two different initiator/accelerator systems: a Raman spectroscopic monitoring, J. Raman Spectrosc. 39, 767-771.

Maier S. A., 2007, Plasmonics: Fundamentals and Applications, Springer.

Marchisio D. L., Rivautella L., Barresi A. A., 2006, Design and Scale-Up of Chemical Reactors for Nanoparticle Precipitation, AIChE J 52, 1877-1887.

Merhari L., Ed., 2009, Hybrid Nanocomposite for Nanotechnology: Electronic, Optical, Magnetic and Biomedical Applications, Springer.

Mazerolles L., Michel D., Vignes J-L., di Costenzo, Huang Z., Jiang D., 2003, Nanostructured materials based on alumina, Ceramic Eng. Sc. Proceed. 24, 105-111.

Morfa, A. J., Rowlen K. L., Reilly T. H., Romero M. J., van de Lagemaat J., 2008, Plasmon-enhanced solar energy conversion in organic bulk heterojunction Photovoltaics, Appl. Phys. Lett. 92, 013504.

Rivallin M., Benmami M., Kanaev A., Gaunand A., 2005a, Sol-gel reactor with rapid micromixing: modelling and measurements of titanium oxide nano-particles growth, Chemical Engineering Research & Design, 83(A1), 67-74.

M. Rivallin, M. Benmami, A. Gaunand, and A. Kanaev, 2005b, Temperature dependence of the titanium oxide sols precipitation kinetics in the sol-gel process, Chem. Phys. Lett. 398, 157-162.

Rodriguez J. A. and Fernandez-Garcia M. (Ed.), (2007), *Synthesis, Properties, and Applications of Oxide Nanomaterials* (Wiley).

Sanchez C., Rozes L., Ribot F., Laberty-Robert C., Grosso D., Sassoye C., Boissiere C., Nicole L.R., 2010, "Chimie douce": A land of opportunities for the designed construction of functional inorganic and hybrid organic-inorganic nanomaterials", Comptes Rendus Chimie, 13, 3-39.

Soloviev A., Jensen H., Søgaard E.G., Kanaev A.V., 2003, Aggregation Kinetics of Sol-Gel Process based on Titanium Isopropoxide, J. Mater. Sci., 38, 3315-3318.

Thakur R. K., Vial Ch., Nigam K. D. P., Nauman E. B., Djelveh G., 2003, Static mixers in the process industries - A review, Trans IChemE 81A, 787-826.

Tieng S., Azouani R., Chhor K., Kanaev A., 2011a, Nucleation-growth of TiO_2 nanoparticles doped by acetylacetonate: sol-gel route for preparation of photocatalytically active nanocoatings, J. Phys. Chem. C 115, 5244-5250.

Tieng S., Chhor K., Kanaev A., 2011b, New homogeneously doped Fe(III)-TiO_2 photocatalyst for gaseous pollutant degradation, Appl. Catalysis A: General, 399, 191-197.

Vignes J-L., Michel D., Mazerolles L., Frappart C, di Costenzo T., Beauvy M., Patent n° FR2847569 of 28-05-2004 (CNRS-CEA, France).

Vignes J-L., Frappart, di Costenzo T., Rouchaud J-C., Mazerolles L., Michel D., 2008, Ultraporous monoliths of alumina prepared at room temperature by aluminium oxidation, J. Mater. Sci. 43, 1234-1240.

Zhang H.,. Banfield J. F, 1998, Thermodynamic analysis of phase stability of nanocrystalline titania, J. Mater. Chem. 8, 2073-2076.

Zhang H., Banfield J. F., 2000, Understanding polymorphic phase transformation behavior during growth of nanocrystalline aggregates: insights from TiO_2, J. Phys. Chem. B 104, 3481-3487.